



New photolytic converter for improving aircraft measurements of NO₂ via chemiluminescence.

Clara M. Nussbaumer¹, Uwe Parchatka¹, Ivan Tadic¹, Birger Bohn², Daniel Marno¹, Monica Martinez¹, Roland Rohloff¹, Hartwig Harder¹, Flora Kluge³, Klaus Pfeilsticker³, Florian Obersteiner⁴, Martin Zöger⁵, Raphael Doerich¹, John N. Crowley¹, Jos Lelieveld^{1,6}, and Horst Fischer¹

¹Max Planck Institute for Chemistry, Department of Atmospheric Chemistry, 55128 Mainz, Germany

²Institute of Energy and Climate Research, IEK-8: Troposphere, Forschungszentrum Jülich GmbH, 52428 Jülich, Germany

³Institute of Environmental Physics, Heidelberg University, 69120 Heidelberg, Germany

⁴Karlsruhe Institute of Technology, 76021 Karlsruhe, Germany

⁵Flight Experiments, German Aerospace Center (DLR), 82234 Oberpfaffenhofen, Germany

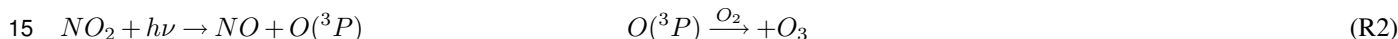
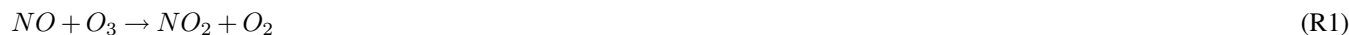
⁶Climate and Atmosphere Research Center, The Cyprus Institute, Nicosia, Cyprus

Correspondence: Clara M. Nussbaumer (clara.nussbaumer@mpic.de)

Abstract. Nitrogen oxides (NO_x ≡ NO + NO₂) are centrally involved in the photochemical processes taking place in the earth's atmosphere. Measurements of NO₂, particularly in remote areas where concentrations are of the order of pptv (parts per trillion by volume), are still a challenge and subject to extensive research. In this study, we present NO₂ measurements via photolysis-chemiluminescence during the research aircraft campaign CAFE Africa (Chemistry of the Atmosphere - Field Experiment in Africa) 2018 around Cabo Verde as well as the results of laboratory experiments to characterize the photolytic converter used. We identify a memory effect within the conventional photolytic converter associated with high NO concentrations and rapidly changing water vapor concentrations, accompanying changes in altitude during aircraft measurements, which is due to the porous structure of the converter material. We test and characterize an alternative photolytic converter made from quartz glass which improves the reliability of NO₂ measurements in laboratory and field studies.

10 1 Introduction

NO_x (nitrogen oxides) represent the sum of NO (nitric oxide) and NO₂ (nitrogen dioxide) which can rapidly interconvert in the atmosphere in the presence of sunlight and O₃ (ozone) as shown in Reactions (R1) and (R2) (Jacob, 1999).



Considering only these two reactions in atmospheric NO_x chemistry, the so called Leighton ratio represents NO₂, NO and O₃ in photostationary state (PSS) as shown in Equation (1) (Leighton, 1961). k_{NO+O_3} is the rate coefficient of Reaction (R1) and



j_{NO_2} is the photolysis frequency for NO_2 in Reaction (R2).

$$\frac{k_{NO+O_3} \times [NO] \times [O_3]}{j_{NO_2} \times [NO_2]} = \phi \approx 1 \quad (1)$$

20 Several studies have shown that the Leighton ratio as presented in Equation (1) is only valid for highly polluted environments whereas in other regions, besides O_3 , oxidized halogen species and peroxy radicals (HO_2 and RO_2) significantly contribute to the oxidation of NO to NO_2 and require an extension of the Leighton expression for a reliable calculation of PSS NO_2 concentrations as presented in Sect. 2.4. (Mannschreck et al., 2004; Griffin et al., 2007; Ma et al., 2017; Reed et al., 2016).

NO_x can be emitted from either natural and anthropogenic sources, with the latter dominating globally. Natural emissions
25 include for example biogenic soil emissions, biomass burning and lightning. Anthropogenic emissions are mainly from combustion processes in vehicles or from power and industrial plants which contribute almost two thirds to the global burden (Pusede et al., 2015; Ganzeveld et al., 2002; Logan, 1983). Nitrogen oxides are, together with volatile organic compounds, important precursors to tropospheric ozone which can be a hazard to plant, animal and human health, causing multiple diseases regarding the cardiovascular and respiratory system (Nussbaumer and Cohen, 2020; Nuvolone et al., 2018; Lippmann, 1989).
30 NO_x additionally promote the formation of acid rain (through conversion to HNO_3) - hazardous to many ecosystems - and are a threat to human health themselves (Boningari and Smirniotis, 2016; Greaver et al., 2012). Beyond that, NO_x control the abundance of OH radicals which regulate the oxidizing capacity of the atmosphere (Levy, 1971; Lelieveld and Dentener, 2000). Due to the health implications and the impact on atmospheric photochemical processes, it is highly relevant to measure and monitor ambient NO_x concentrations with sophisticated instruments which provide reliable concentration measurements,
35 especially also in remote areas where NO and NO_2 are low. More specifically, this requires a low instrumental background which - particularly for NO_2 - is often impacted by unwanted chemical processes which can lead to artifact signals (Reed et al., 2016; Andersen et al., 2020; Jordan et al., 2020).

Many different measurement techniques have been deployed to measure nitrogen oxides such as cavity enhanced absorption spectroscopy (and variants, e.g. cavity attenuated phase shift spectroscopy (Ge et al., 2013; Keabian et al., 2005), cavity ring
40 down spectroscopy (O'Keefe and Deacon, 1988) and others (Zheng et al., 2018)), differential optical absorption spectroscopy (Hüneke et al., 2017; Winer and Biermann, 1994) and laser induced fluorescence (Thornton et al., 2000; Javed et al., 2019) for NO_2 or absorption spectroscopy for NO (Ventrillard et al., 2017). However, detection of NO and NO_2 via chemiluminescence (CLD) is likely the most common technique for the measurement of nitrogen oxides in the atmosphere and is distinguished by the simultaneous in-situ measurement of both, NO and NO_2 , low detection limits and the deployability in research aircrafts
45 at high altitudes for measurements in the upper troposphere (Pollack et al., 2010; Reed et al., 2016; Tadic et al., 2020). The measurement principle is based on the reaction of nitric oxide and ozone which yields electronically excited NO_2 (NO_2^*) which (along with physical quenching) returns to the electronic ground state by fluorescence whereby a photon of a wavelength > 600 nm is emitted, which can be detected by a photomultiplier tube. The resulting signal is proportional to the initial NO concentration (Clough and Thrush, 1967). For nitrogen dioxide detection, NO_2 is first converted to NO . The standard method
50 for this conversion is the use of a catalytic converter, in which NO_2 passes through a heated molybdenum converter where it is reduced by Mo to NO ($Mo + 3 NO_2 \rightarrow MoO_3 + 3 NO$). However, high temperatures ($300 - 350^\circ C$) in the converter along with



catalytic surface effects lead to interferences with other atmospheric compounds that can be converted to NO₂ such as HONO (nitrous acid), HNO₃ (nitric acid) or PAN (peroxyacyl nitrate) and bias the measurement (Demerjian, 2000; Villena et al., 2012; Jung et al., 2017). An alternative and widespread method is the use of a photolytic converter (photolysis-chemiluminescence: P-CL), also referred to as blue light converter, which utilizes LEDs emitting at a wavelength of around 395 nm to dissociate NO₂ to NO (Pollack et al., 2010; Reed et al., 2016; Tadic et al., 2020; Ryerson et al., 2000). Interferences (as described above) in the blue light converter are still possible, but to a significantly lesser extent. Reed et al. (2016) investigated potential interferences in a photolytic converter which are related to the presence of PAN, methyl peroxy nitrate (MPN, CH₃O₂NO₂) or pernitric acid (PNA, HO₂NO₂). These compounds are NO₂ reservoir species and their decomposition (to NO₂) is dependent on the temperature, the pressure and the residence time in the blue light converter (Nault et al., 2015; Fischer et al., 2014). Please note, that none of these compounds are photolyzed in the blue light converter and only subject to thermal decomposition (Reed et al., 2016; Tadic et al., 2020). Generally, increasing temperature and residence time promote the decay of thermally unstable trace gases and the release of NO₂ which is further described in Section 2.5 (Reed et al., 2016). The CLD detects a signal (which we call NO_c signal) which is composed of the ambient NO concentration and the ambient NO₂ concentration multiplied by the conversion efficiency C_e according to Equation (2).

$$[NO_c] = [NO] + C_e \times [NO_2] \quad (2)$$

The conversion efficiency describes the fraction of NO₂ that is converted to NO in the converter and can be thought of as the NO yield from NO₂. Its value is dependent on the optical output of the LEDs as well as the NO₂ residence time and the pressure in the converter. C_e is therefore in competition with unwanted formation of NO₂ from NO₂ reservoir species. For example, a longer residence time increases the conversion efficiency, but could potentially increase the amount of NO₂ reservoir species that decay in the converter, which takes place according to first order kinetics which is described in more detail in Section 2.5. The NO₂ concentration is calculated from the difference in the signal with and without use of the photolytic converter: $[NO_2] = ([NO_c] - [NO]) / C_e$ (Sadanaga et al., 2010; Tadic et al., 2020; Ryerson et al., 2000).

While NO measurements are generally reliable and well-understood, NO₂ measurement techniques utilizing the conversion of NO₂ to NO are subject to extensive research. Hosaynali Beygi et al. (2011) found a strong deviation from the Leighton ratio at low NO_x concentrations between 5 and 25 pptv despite the inclusion of HO₂, RO₂ and halogen oxides suggesting the occurrence of a so far unknown atmospheric oxidant. Frey et al. (2015) also reported higher measured NO₂/NO ratios than expected from PSS based on measurements in Antarctica and hypothesized the presence of an additional oxidant or a measurement bias. This is in line with findings and suggestions by Silvern et al. (2018) based on observations during the aircraft campaign SEAC⁴RS over the United States of America. Reed et al. (2016) examined the described deviation through the laboratory investigation of potential NO₂ interferences of thermally unstable trace gases such as peroxyacyl nitrate (PAN) within the photolytic converter in comparison to laser-induced fluorescent NO₂ measurement and found that this could contribute to the higher than expected NO₂ concentrations measured by P-CL instruments. Jordan et al. (2020) investigated interferences in a photolytic converter made from quartz glass and showed how the converter conditions affect the conversion efficiency and the



85 artifact signal (caused by NO₂ reservoir species). The correct adjustment of the conditions, preferably including low pressure,
high flow rates and small temperature variations, can minimize interferences. Andersen et al. (2020) reported the measurement
of a significant NO₂ measurement bias during ground-based observations in the remote marine tropical troposphere with a con-
ventional blue light converter which was related to its porous walls. They were able to eliminate this effect by implementation
of a photolytic converter made from quartz glass which reduced the overall measurement uncertainty by around 50 %.

90 An additional challenge is the significant decrease in the NO₂/NO ratio with altitude. At the surface at daytime, NO₂ concen-
trations are approximately two to four times higher than NO concentrations. The NO₂/NO ratio decreases by around one order
of magnitude when going from the lower to the upper troposphere which increases the uncertainty when deriving NO₂ mixing
ratios using Equation (2) (Travis et al., 2016; Silvern et al., 2018; Logan et al., 1981). At the same time, the concentration of
NO₂ reservoir species such as PNA or MPN is significantly higher in the upper troposphere compared to that at the surface and
95 consequently interferences are more likely to occur at high altitudes (Nault et al., 2015; Kim et al., 2007). These aspects result
in particularly strict requirements regarding airborne NO₂ measurements.

In this study, we describe a modified blue light converter (BLC) originally purchased from Droplet Measurement Technolo-
gies, which we have deployed in NO₂ measurements via photolysis-chemiluminescence during the research aircraft campaign
CAFE Africa (Chemistry of the Atmosphere: Field Experiment in Africa) and also in laboratory investigations. We show how
100 high NO concentrations and rapidly changing water vapor concentrations affect the instrumental background and induce a
memory effect which cannot be corrected retrospectively. This is particularly relevant to aircraft measurements where water
vapor concentrations are subject to rapid changes due to variations in flight altitude, but also to all other application areas. The
photolytic converter and similar designs are widely used for field measurements of NO₂ all across the world (e.g. Andersen
et al. (2020); Jung et al. (2017); Xu et al. (2013); Breuninger et al. (2013); Fuchs et al. (2010); Reidmiller et al. (2010); Crowley
105 et al. (2010); Sather et al. (2006)) and can provide reliable results for stationary use and locations with only little variations in
ambient NO and low humidity levels, but suffer from enhanced uncertainty in other applications. We propose the elimination
of any direct contact points between the sample gas and the porous inner converter surface and have developed an alternative
photolytic converter entirely made from quartz glass. Highly reflective properties are achieved by an outer mantel made from
optical PTFE (polytetrafluoroethylene, also known as teflon). The new converter shows promising results in the laboratory
110 regarding its application in field studies for more reliable NO₂ measurements. We do not claim to be the first to present an
alternative quartz glass converter for P-CL measurement of NO₂. However, we are first to point out the technical difficulties in
the application of conventional NO₂ converters in airborne studies and believe the presented results to be a guidepost for future
NO₂ aircraft measurements via photolysis-chemiluminescence.

2 Observations and methods

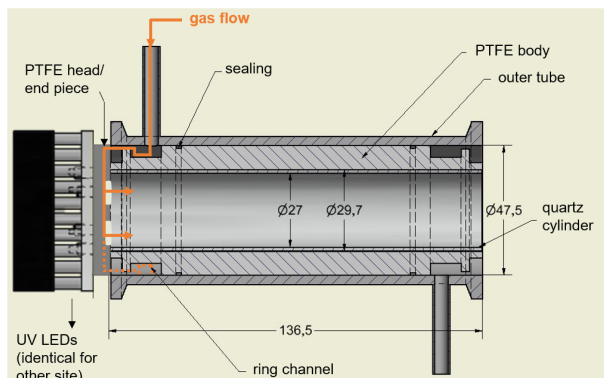
115 2.1 Instrument

All NO_x measurements were performed using a modified commercially available two-channel chemiluminescence instrument
(detector from ECO Physics CLD 790 SR, Dürnten, Switzerland) as described by Tadic et al. (2020) operated at a total gas flow

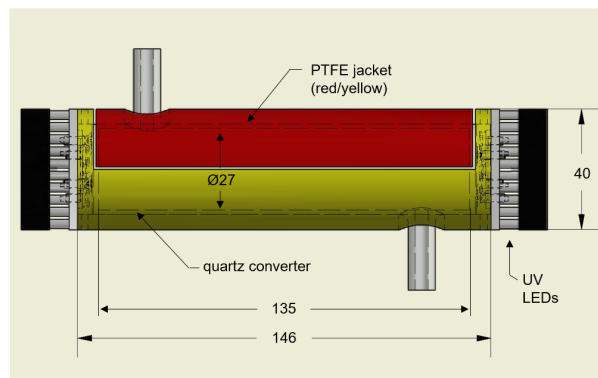


of 3 SLM, equally divided into the two channels. NO concentrations are measured in the first channel, also referred to as the NO channel, through formation of NO_2^* via reaction with O_3 . The resulting excited NO_2^* emits a photon ($> 600 \text{ nm}$) detected
120 by a photomultiplier tube, preamplifier set up and recorded as counts per second. The second channel, also referred to as NO_c
channel, is structurally identical except for the implementation of a photolytic converter which converts a known fraction of
 NO_2 to NO prior to the reaction with O_3 and is operated at a constant pressure of 110 hPa (105 hPa during the CAFE Africa field
experiment). NO_2 concentrations are obtained from the difference in counts from each channel and the conversion efficiency
 C_e as described above (see Equation 2). We use a blue light converter purchased from Droplet Measurement Technologies
125 equipped with UV-LEDs emitting at a wavelength of 398 nm (FWHM = 16 nm) which is shown in Figure 1a (Tadic et al.,
2020). Originally, the inner material is made of porous, optically active PTFE (polytetrafluoroethylene) for providing highly
reflective properties. To reduce surface effects the converter was equipped with a quartz cylinder covering approximately half
of the PTFE surface (the gas still gets in touch with the PTFE surface in the ring channel and through the head piece). The
sample gas enters the converter sideways into the ring channel and reaches the inner tube via the PTFE head piece which has
130 four circular recesses, one for each UV LED. The sample gas outlet proceeds analogously. The inner volume of the converter is
 $V = 78 \text{ cm}^3$ which gives a residence time of $t = \frac{V \times 60 \text{ s min}^{-1}}{F} \times \frac{p}{p_{\text{standard}}} = \frac{78 \text{ cm}^3 \times 60 \text{ s min}^{-1}}{1500 \text{ cm}^3 \text{ min}^{-1}} \times \frac{110 \text{ hPa}}{1013 \text{ hPa}} = 0.34 \text{ s}$.
The conversion efficiency for this photolytic converter operated under the conditions described above is approximately 20 %
which was determined via gas phase titration (GPT) of NO with ozone. The results obtained with the described blue light
converter were compared to a newly-developed photolytic converter completely made from quartz glass which is shown in
135 Figure 1b. For maintaining the reflective properties of the blue light converter, the new quartz glass converter was jacketed
with optical PTFE which provides diffuse reflectance of $> 99 \%$ in the wavelength range 350 - 1500 nm (SphereOptics GmbH,
2017). The volume of the new converter is 77 cm^3 which gives a residence time of $t = 0.33 \text{ s}$ and a conversion efficiency of
approximately 14 % under the operating conditions. The main difference between the two converters is that the sample gas flow
does not get in direct contact with the porous surface of the material for the new quartz glass converter. The reaction chambers
140 (where the reaction of NO and O_3 takes places) are operated at a constant temperature of $25 \text{ }^\circ\text{C}$ and a pressure of 7 - 8 mbar in
order to minimize quenching of NO_2^* by other molecules. The dry ozone flow is humidified with water vapor for maintaining
a constant humidity level at all times.

Besides the photons emitted from relaxation of NO_2^* , the PMT signal also includes detected photons from interference
reactions, for example the reaction of O_3 with alkenes (Alam et al., 2020), as well as a dark current signal. Therefore, a
145 pre-chamber measurement is operated for 20 seconds every 5 minutes where ozone is added to the sample gas flow. The
residence time in the pre-chamber allows for the reaction of O_3 and NO and the relaxation of NO_2^* before entering the main
reaction chamber. It is not long enough to convert interfering compounds which then occurs in the following main chamber.
Consequently during pre-chamber measurements, the PMT signal only includes the interfering signal and the dark current
signal (Ridley and Howlett, 1974; ECO PHYSICS AG, 2002). We subtracted the interpolated signal obtained during pre-
150 chamber measurements from the signal detected during main chamber measurements in order to obtain the signal generated
from NO.



(a) conventional blue light converter with quartz glass cylinder



(b) new photolytic quartz glass converter

Figure 1. Sketches of the photolytic converters applied in this study.

The instrumental background of each channel is determined via zero (synthetic) air measurements from a gas cylinder and can be converted to mixing ratios using calibration measurements with a known NO concentration which defines the sensitivity (counts s⁻¹ per ppbv (parts per billion by volume) of each channel towards NO as shown in Eq. (3) (after pre-chamber corrections). The signal detected from zero air measurement (counts(zero air)) is subtracted from the signal detected from NO calibration (counts(NO calibration)) and divided by the absolute concentration of the NO calibration (c(NO calibration)) to calculate the sensitivity. Dividing the signal detected from zero air measurements by this value gives the background concentration in mixing ratios, e.g. ppbv.

$$\text{sensitivity} = \frac{\text{counts}(\text{NO calibration}) - \text{counts}(\text{zero air})}{c(\text{NO calibration})} \quad c(\text{background}) = \frac{\text{counts}(\text{zero air})}{\text{sensitivity}} \quad (3)$$

Please note that the utilized zero air can include a trace concentration of NO_x. The manufacturer specifies the maximum concentration of NO_x to be 0.1 ppmv (parts per million by volume) (Westfalen Gas Schweiz GmbH).

2.2 CAFE Africa field experiment

The CAFE Africa research campaign took place in August and September 2018 and included fourteen measurement flights (MF03 - MF16) which were performed with the HALO (High Altitude Long Range) research aircraft starting from the campaign base in Sal on Cabo Verde (16.75 ° N, 22.95 ° W). We included data measured during the measurement flights MF10, MF12, MF13, MF14 and MF15 in this analysis (MF11 was a nighttime flight and therefore excluded) for which CLD NO₂ measurements were available. An overview of the flight tracks is presented in Figure 2. More details on the campaign can be found in Tadic et al. (2021).

NO and NO₂ were measured via photolysis-chemiluminescence with the instrument described in Sect. 2.1 using the conventional blue light converter equipped with the quartz glass cylinder, operated at a temperature of 313 K and a pressure of

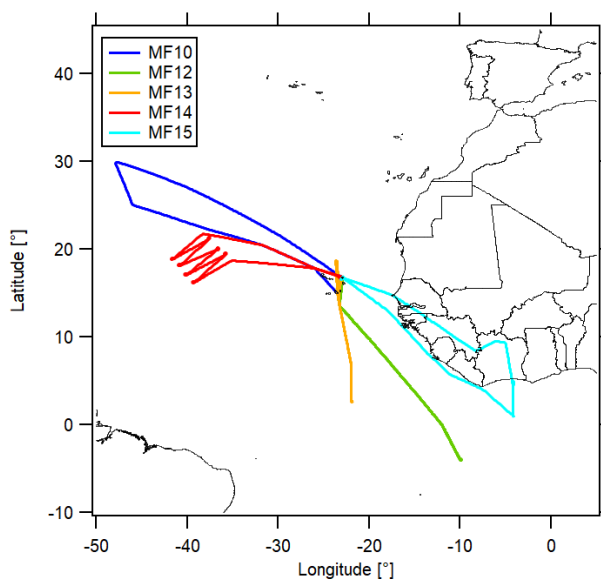


Figure 2. Geographic overview of the measurement flight tracks included in this analysis.

105 hPa (0.32 s residence time). Please note that it was not possible to measure the temperature inside the converter. Instead, the temperature of the gas outflow from the converter in the ring channel was measured which we assume to be identical to the inner temperature. Zero air measurements and NO calibrations were performed regularly to determine the variability in the instrumental background and the sensitivity of the channels. The ambient measurement was interrupted every 1 - 2 h by one
175 minute zero air measurement, followed by one minute NO calibration and another one minute zero air measurement. These calibration-background-cycles (CB-cycles) were performed 4 - 6 times during each measurement flight. We linearly interpolated these background and calibration measurements to each entire flight. The NO data were processed as described by Tadic et al. (2021) (5 pptv detection limit and 6 % relative uncertainty). Please note that the instrumental background for the NO data was determined by nighttime measurements of NO instead of zero air measurements as presented by Tadic et al. (2021) and
180 previously described by Lee et al. (2009). For the NO₂ data, the NO_c channel sensitivity and the background concentration were calculated after pre-chamber correction according to Equation (3). The ambient NO_c signal was divided by the channel sensitivity, accordingly. Final NO₂ concentrations were determined via Equation (4) which includes subtraction of the calculated (and interpolated) NO_c background concentration and the NO concentration in the NO channel, and dividing by the conversion efficiency of the blue light converter which was 24.2 ± 2.8 % during the campaign.

$$185 \quad c(\text{NO}_2) = \frac{c(\text{NO}_c) - c(\text{background}_{\text{NO}_c}) - c(\text{NO})}{C_e} \quad (4)$$



2.3 Further measurements

Additional measurements of atmospheric trace gases during CAFE Africa including O₃, CO, CH₄, HO₂, OH, NO₂ and water vapor as well as the photolysis frequencies j_{NO_2} and j_{PNA} were used in this study. O₃ was measured via UV absorption and chemiluminescence with the FAIRO (Fast AIRborne Ozone) instrument (total measurement uncertainty of 2.5 %, Zahn et al. (2012)). CO and CH₄ were measured via quantum cascade laser absorption spectroscopy (total measurement uncertainty of 4.3 % and 0.3 %, respectively, Schiller et al. (2008)). HO₂ and OH were measured with the custom-built HORUS (HydrOxyl Radical measurement Unit based on fluorescence Spectroscopy) instrument via fluorescence spectroscopy (Novelli et al., 2014; Marno et al., 2020). Please note that these data are still preliminary and the measurement uncertainty is estimated at 50 %. Additional NO₂ concentrations for comparison were measured via differential optical absorption spectroscopy (miniDOAS) with a detection limit of about 5 pptv and an uncertainty depending on the altitude and cloud cover of typically 40 pptv (Hüneke et al., 2017; Kluge et al., 2020). Water vapor was measured via direct absorption by the tunable diode laser system SHARC (Sophisticated Hygrometer for Atmospheric ResearCh) (accuracy of 5 %, detection limit typically in the range of 2 - 3 ppmv) (Kaufmann et al., 2018). The photolysis frequencies were calculated from actinic flux densities measured with a spectral radiometer (Meteorologie Consult GmbH, Metcon, Koenigstein, Germany) (uncertainty < 15 %) (Bohn and Lohse, 2017). Please note that all measurement data were converted to a uniform timescale with a 1 min time resolution as a basis for this analysis.

2.4 NO₂ calculations

For calculating the photostationary state NO₂ concentrations during CAFE Africa, we assume that NO₂ production occurs through reaction of NO with O₃ (Reaction (R1)), HO₂ (Reaction (R3)) and RO₂ (Reaction (R4)). Tadic et al. (2021) showed that RO₂ is well represented by CH₃O₂ during CAFE Africa via model simulations (80 % at 200 hPa altitude and up to 90 % below) which we therefore use as surrogate for describing all organic peroxy radicals. In analogy to Leighton (1961), we describe NO₂ loss by photo dissociation as shown in Reaction (R2). Other loss pathways for NO₂ for example via OH can be neglected (< 1 %) (Bozem et al., 2017).



210



NO₂ concentration in photostationary state can therefore be obtained via Equation (5) whereas the concentration of CH₃O₂ is calculated by help of Equation (6) which was derived by Bozem et al. (2017). For the calculation via Equation (6) we assume that CH₃O₂ and HO₂ formation occur through CH₄ and CO oxidation, respectively. We estimate an uncertainty of around 20 % resulting from these assumptions. Propagating the measurement uncertainties of HO₂, CH₄ and CO suggests a 50 % uncertainty

215



in the calculated CH_3O_2 data. The NO_2 PSS data have an uncertainty of 22 % regarding the trace gas measurements according to Gaussian error propagation (uncertainty of rate coefficients is considered negligible).

$$[\text{NO}_2]^{PSS} = \frac{[\text{NO}] \times (k_{\text{NO}+\text{O}_3} \times [\text{O}_3] + k_{\text{NO}+\text{HO}_2} \times [\text{HO}_2] + k_{\text{NO}+\text{CH}_3\text{O}_2} \times [\text{CH}_3\text{O}_2])}{j_{\text{NO}_2}} \quad (5)$$

$$220 \quad [\text{CH}_3\text{O}_2] = \frac{k_{\text{CH}_4+\text{OH}} \times [\text{CH}_4]}{k_{\text{CO}+\text{OH}} \times [\text{CO}]} \times [\text{HO}_2] \quad (6)$$

The temperature dependent rate coefficients were obtained from the data sheets of the IUPAC Task Group on Atmospheric Chemical Kinetic Data Evaluation (2021) (Atkinson et al., 2004, 2006).

2.5 Calculation of NO_2 reservoir species

We consider the NO_2 reservoir species PAN, MPN and PNA. PAN was measured during CAFE Africa via chemical ionization
225 mass spectrometry (CIMS) (Phillips et al., 2013). MPN and PNA were not measured and instead estimated via photostationary
state calculations as suggested by Murphy et al. (2004). PNA (HO_2NO_2) production occurs through reaction of HO_2 and NO_2
(R5) while PNA loss is described by Reactions (R6)-(R8) either through thermal decomposition, photolysis or reaction with
OH (Veres et al., 2015; IUPAC Task Group on Atmospheric Chemical Kinetic Data Evaluation, 2021; Atkinson et al., 2004).
PSS HO_2NO_2 concentrations can then be calculated via Equation (7). k is the rate coefficient for each reaction and j_{PNA} is
230 the photolysis frequency for Reaction (R7).



$$[\text{HO}_2\text{NO}_2]^{PSS} = \frac{k_5 \times [\text{HO}_2][\text{NO}_2]^{PSS}}{k_6 + j_{\text{PNA}} + k_8 \times [\text{OH}]} \quad (7)$$

240 MPN production and loss terms are in analogy to PNA as shown in Reactions (R9)-(R11) except for the reaction with OH
which is negligible (Nault et al., 2015; Browne et al., 2011; Murphy et al., 2004; Bahta et al., 1982). The calculation in PSS is



performed via Equation (8). k represents the rate coefficients and j_{MPN} is the photolysis frequency for Reaction (R11). During CAFE Africa, only the photolysis frequency j_{PNA} was evaluated because reliable molecular data for MPN were missing. As suggested by Murphy et al. (2004) we assume identical UV cross sections of MPN and PNA and therefore j_{MPN} to be identical
 245 with j_{PNA} .



$$[CH_3O_2NO_2]^{PSS} = \frac{k_9 \times [CH_3O_2][NO_2]^{PSS}}{k_{10} + j_{MPN}} \quad (8)$$

In the photolytic converter PNA, MPN and PAN can decompose to NO_2 depending on the temperature, the pressure and the residence time t according to first order kinetics. The resulting NO_2 artifact is determined via Equation (9).

255
$$[NO_2]_{artifact} = [HO_2NO_2]^{PSS} \times (1 - \exp(-k_6 \times t))$$

$$+ [CH_3O_2NO_2]^{PSS} \times (1 - \exp(-k_{10} \times t)) \quad (9)$$

$$+ [CH_3COO_2NO_2] \times (1 - \exp(-k_{CH_3COO_2NO_2+M} \times t))$$

Gaussian error propagation gives an uncertainty of 55 % for the calculated PNA and MPN data. We use the residence time according to the volume and the flow rate in the photolytic converter as described earlier. The actual value could deviate from the calculated one due to unknown flow-dynamics and temperature gradients. Assuming 30 % uncertainty in the residence time gives an overall uncertainty of around 60 % in the NO_2 formed from PNA and MPN in the photolytic converter.

260 3 Results and Discussion

3.1 Aircraft measurements

3.1.1 NO_2 reservoir species

Figure 3a shows the vertical concentration profiles of the NO_2 reservoir species MPN and PNA according to photostationary steady state calculations (Equations (8) and (7)) as well as PAN measurements during CAFE Africa. MPN concentrations were

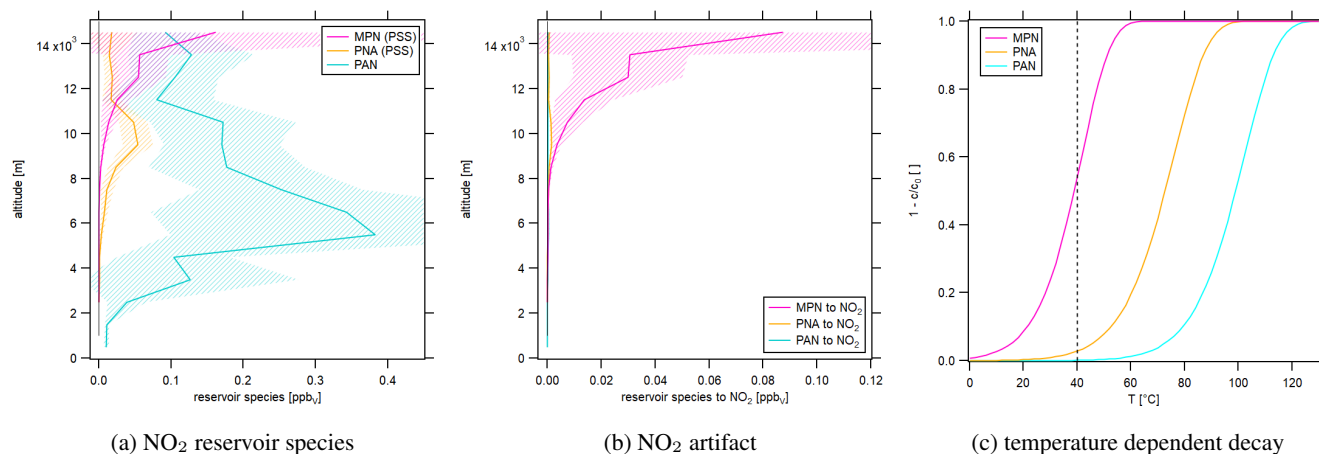


Figure 3. Vertical profiles of (a) NO₂ reservoir species MPN, PNA (from PSS calculations) and PAN (measured during CAFE Africa) and (b) NO₂ artifacts in the blue light converter from reservoir species according to first order decay. The shaded plot areas present the 1 σ standard deviation resulting from averaging the concentrations at each considered altitude range. (c) Temperature dependent decay of the NO₂ reservoir species in the blue light converter.

265 close to zero at low altitudes up to 10 km and increased above, reaching 57 ± 40 pptv between 13 and 14 km altitude. The concentration increased further aloft but had a large variability. PNA mixing ratios were low below 8 and above 12 km altitude and showed peak concentrations of 54 ± 21 pptv between 9 and 10 km. PAN increased from ground level to mid-range altitudes with a maximum of 383 ± 283 pptv at 4 - 5 km. Concentrations subsequently decreased with altitude, reaching 92 ± 44 pptv at 14 - 15 km. Figure 3b shows the NO₂ artifact concentrations resulting from thermal decomposition of the reservoir species in
 270 the blue light converter according to first order decay. It can be seen that only relevant artifact signals originated from MPN of which more than 50 % decomposed to NO₂ at the conditions present in the converter. 3 % of the ambient PNA was converted to NO₂. Even though atmospheric PAN concentrations, particularly at mid-range altitudes, were high, temperature, pressure and residence time in the blue light converter were too low for PAN to decay to NO₂. As an overview, Figure 3c shows the temperature-dependent decay ($1 - c/c_0$) of the discussed NO₂ reservoir species in the converter. The calculation is based on
 275 constant pressure (105 hPa) and residence time (0.32 s). The temperature in the converter is shown with the black dashed line. Increasing temperature increases the decomposition share. It can be seen that, for PAN and PNA, the converter temperature would need to be significantly higher to observe a relevant decay (10 % decay of PNA at $> 50^\circ \text{C}$ and of PAN at $\sim 80^\circ \text{C}$). In contrast for MPN, small changes in the temperature have a strong effect on the decomposing share (4 % per $^\circ \text{C}$ at the steepest point). We show the time- and pressure-dependent decay of PAN, PNA and MPN in Figure S1 of the Supplement. PAN and
 280 PNA decay only slightly depends on pressure at the given temperature and residence time. Please note that the residence time and the pressure are correlated, which we have neglected in this calculation. Based on these results, we recommend the implementation of a monitoring system for pressure and, more importantly, temperature within the photolytic converter which

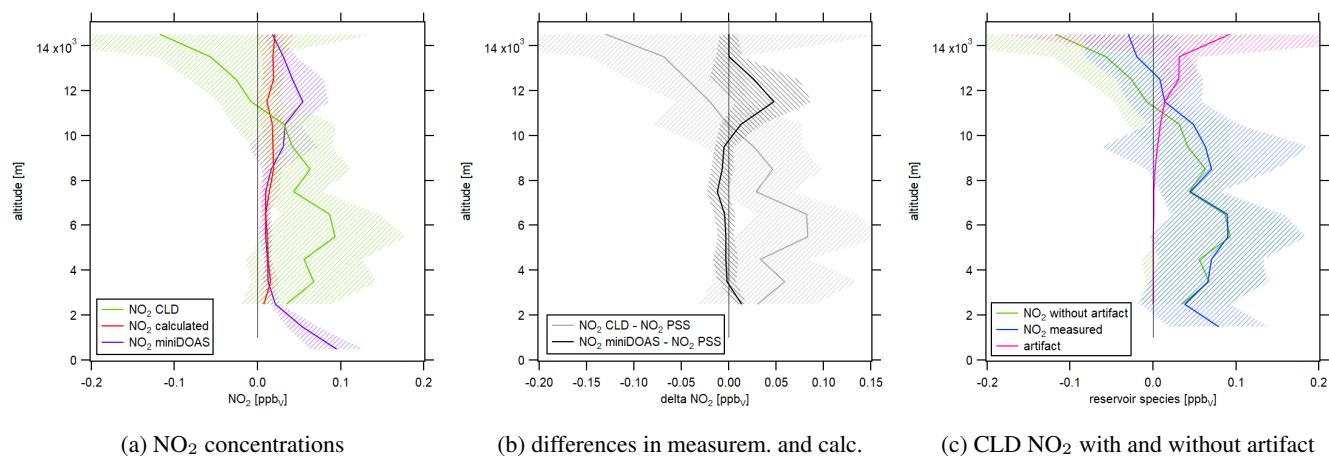


Figure 4. Vertical profiles of (a) NO_2 concentrations measured by the CLD, miniDOAS and calculated via Eq. (5), (b) the difference in NO_2 concentrations from PSS calculations and measurements and (c) CLD NO_2 concentrations with and without artifact. The shaded plot areas present the 1σ standard deviation resulting from averaging concentrations at each considered altitude range.

is difficult to implement in the commercially available blue light converter, but allows for a more accurate calculation of the decomposing share and consequently a reliable correction of the NO_2 signal.

285 We have subtracted the NO_2 artifact signal arising from the decomposition of MPN and PNA from the CLD NO_2 concentrations. Please note that the data coverage for the NO_2 artifact from MPN is 55 % and from PNA is 48 % (difference due to OH data coverage). We have interpolated the data used in the following sections to reach full coverage of the CLD NO_2 concentrations. Sometimes the data were incomplete at the start or the end of a measurement flight in which case we considered the averaged NO_2 artifact signal according to the vertical profile shown in Figure 3b as a function of the altitude.

290 3.1.2 Atmospheric NO_2 concentrations

Figure 4 shows the vertical profile of NO_2 concentrations measured via CLD in green, miniDOAS measurements in purple and NO_2 from PSS calculations in red. Calculated PSS NO_2 concentrations were on average 17 ± 14 pptv and approximately constant over the considered altitude range. At high altitudes, NO_2 from decomposing reservoir species exceeded the PSS values by around a factor of five. NO_2 concentrations measured by the miniDOAS instrument were 95 ± 31 ppt at ground level and decreased with altitude up to 2 km. They were constant with 15 ± 16 pptv between 2 and 10 km altitude and agreed to within $\sim 85\%$ to the calculated values. Concentrations increased again above reaching 54 ± 31 pptv between 11 and 12 km and decreased aloft with values similar to PSS NO_2 between 14 and 15 km. Average NO_2 concentrations measured by the CLD were 49 ± 76 pptv below 10 km altitude where decomposition of reservoir species did not play a role and decreased with altitude above. Figure 4b shows the calculated difference in NO_2 concentrations between PSS calculations and miniDOAS measurements in black, and between PSS calculations and CLD measurements in gray. It is notable that NO_2 concentrations from PSS and miniDOAS measurements were nearly identical apart for a difference with a maximum value of 48 ± 4 pptv

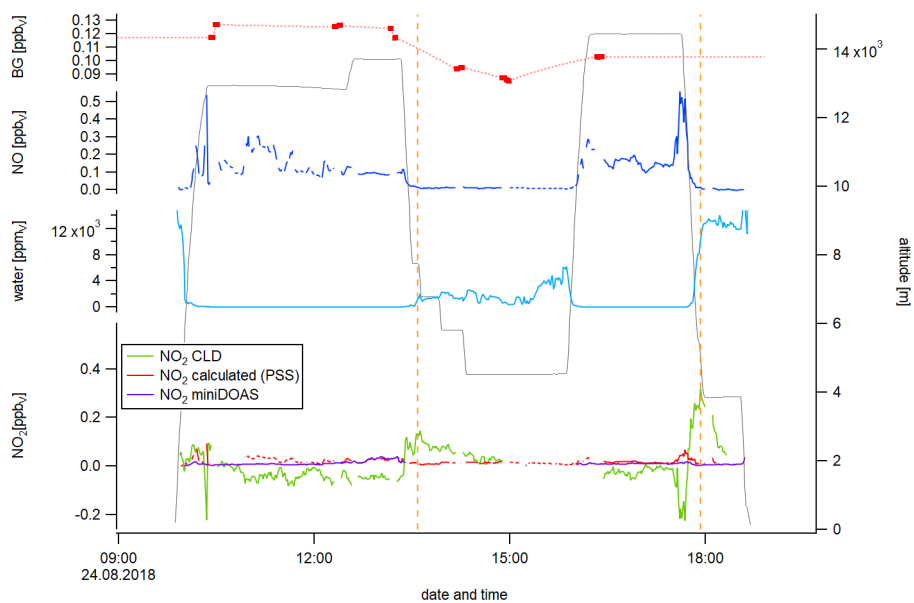


between 10 and 13 km altitude. In contrast, CLD NO₂ concentrations were higher by 45 ± 62 pptv compared to the calculation up to 10 km altitude and lower at higher altitudes with a maximum deviation of more than 100 pptv between 14 and 15 km. Figure 4a shows that the NO₂ CLD mixing ratios are negative at high altitudes. This is an indicator of a wrongly measured background signal in the second channel. If the determined instrumental background was too high, Eq. (4) could return underestimated or even negative NO₂ concentrations. However, the CLD NO₂ data were not generally too small, but even enhanced at lower altitudes compared to PSS and miniDOAS data which may indicate the contribution of additional factors which we investigate in the following by the help of NO, H₂O and NO₂ concentrations in the course of selected measurement flights. For comparison, Figure 4c shows the CLD NO₂ data with and without the calculated artifact signal. It can be seen that the data are already negative before the subtraction of decomposing NO₂ reservoir species.

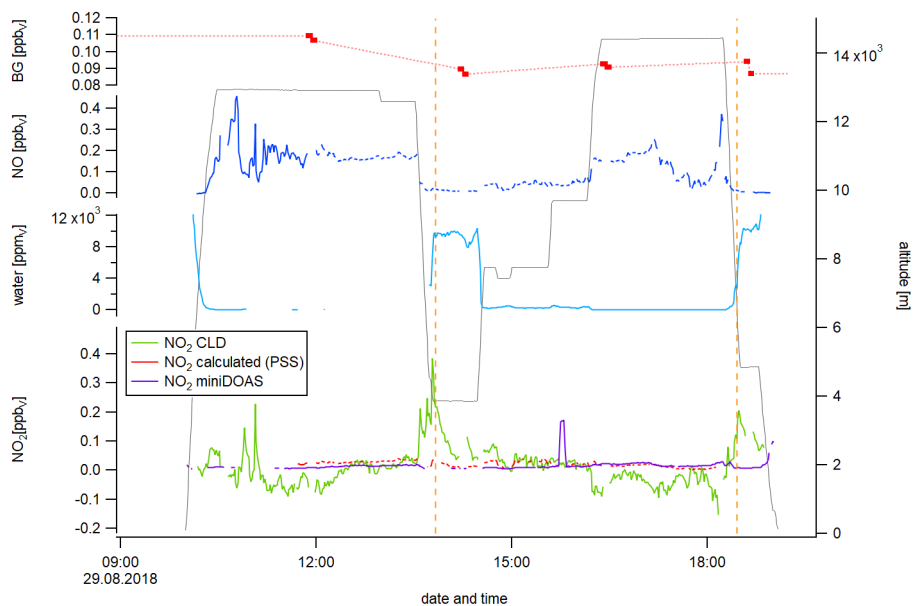
3.1.3 Influence of atmospheric water vapor

Atmospheric water vapor concentrations are highest at ground-level and decrease with increasing altitude. As an example, the vertical concentration profile of atmospheric water vapor during CAFE Africa is shown in Figure S2 of the Supplement. Accordingly, altitude changes during aircraft measurements introduce rapid changes in relative humidity to the instruments on-board.

Figure 5 shows a time series of NO, water vapor, and calculated and measured NO₂ concentrations during the measurement flights MF10 (Figure 5a) and MF12 (Figure 5b). NO concentrations varied between 0.005 and 0.56 ppbv for MF10 and between 0.005 and 0.46 ppbv for MF12. We have recently shown that enhanced NO concentrations in the morning and afternoon of MF12 were due to local, recent lightning activity (Nussbaumer et al., 2021). For MF10, enhanced NO concentrations at high altitudes had their source over the African continent. At low altitudes, NO concentrations were close to zero as there were no significant NO emissions in the marine boundary layer. Water vapor concentrations showed the expected inverse correlation with the flight altitude with mixing ratios below the detection limit at high altitudes. As already suggested by the vertical NO₂ concentration profiles in Figure 4a, NO₂ concentrations obtained from CLD measurements were lower than NO₂ concentrations from miniDOAS measurements and PSS calculations (and sometimes even below zero) at high altitudes and higher at low altitudes. Please note that the CLD NO₂ data shown in Figure 5 were processed as described earlier. This includes the interpolation of the background and calibration measurements which were performed 6 times for MF10 and 4 times for MF12. A potential variation of the background or the sensitivity of the channels between two CB-cycles would therefore be unaccounted for. We show the background measurements in the top data trace of each subfigure in Figure 5 by red dots and the interpolation as red dashed line. For MF10, the measured background in the NO_c channel varied between 85 and 110 pptv and for MF12 between 87 and 109 pptv. Calculated PSS NO₂ concentrations ranged between 1 and 93 pptv for MF10 and between 2 and 46 pptv for MF12. Local maxima mainly accompanied peaks of nitric oxide which is a result of the NO dependence of Equation (5). NO₂ concentrations measured by the miniDOAS instrument varied between 2 pptv and 39 pptv for MF10. For MF12, concentrations were 15 ± 16 pptv and generally lower for low altitudes and higher for high altitudes. NO₂ concentrations measured by the CLD instrument ranged from -224 to 317 pptv for MF10 and from -153 to 384 pptv for MF12. It is striking that the maxima were obtained simultaneously with a sharp decrease in altitude accompanied by an increase in water vapor



(a) MF10



(b) MF12

Figure 5. Temporal development of NO, water vapor, and calculated and measured NO₂ exemplarily for measurement flights 10 and 12.

concentration. For each measurement flight here shown, this phenomenon was observed twice, indicated by the orange dashed lines. For example, the research aircraft descended from 12.6 km to 3.9 km at 13:30 UTC during MF12. At the same time, the CLD NO₂ concentration increased from an average of 23 ± 14 pptv between 13:00 and 13:30 UTC to its maximum of 384 pptv



at 13:45 UTC when reaching the new lower flight altitude. Water vapor measurements were incomplete before 13:00 UTC, but
340 it can be assumed that they were constant and close to zero at 12.6 km altitude, rising to $9.5 \pm 0.7 \times 10^3$ ppmv on average after
reaching 3.9 km (+ 15 minutes). Similar observations were made for MF12 at 18:30 UTC and for MF10 at around 13:30 and
18:00 UTC, in each case accompanied by a decrease in altitude and an increase in water vapor concentrations. The observed
NO₂ peaks appeared only for the CLD measurement, and not for the values from PSS calculation or miniDOAS measurement
which underlines the instrumental cause. The time series for the measurement flights MF13, MF14 and MF15 shows similar
345 results and can be found in Figure S3 of the Supplement.

We hypothesize that these observations were influenced by a surface effect in the blue light converter which has a highly
porous inner surface as described earlier. This material can adsorb atmospheric compounds, such as NO, and desorb them at a
later stage (for example supported by an increase in humidity), which we will refer to as memory effect in the following. In a
series of laboratory studies, we have investigated the impact of NO concentrations and humidity on the effects described above
350 and particularly in regard to the instrumental background.

3.2 Laboratory experiments and implications for CAFE Africa

We propose that the memory effect described in the previous section is strongly affected by NO molecules and is dependent on
changes in the introduced relative humidity. In order to show this, we have conducted different experiments in the laboratory
to investigate the instrumental background produced by the photolytic converter in the NO_c channel. Beside NO and H₂O, we
355 suggest that one or more additional factors affect the observed background signal which are connected to the light of the LEDs
and which we discuss at the end of this section.

For the first set of experiments, we exposed the converter (LEDs switched-on) to 16 ppbv of NO for 2 h followed by 4 h
zero air measurements. The first experiment was carried out under dry conditions, sampling NO and zero air directly from
the gas cylinder. For the second experiment, we introduced water vapor by passing zero air through a washing bottle with
360 deionized water before entering the instrument. The thus obtained relative humidity was $\sim 95\%$ at ambient temperature and
decreased over time with decreasing water temperature (through evaporation). For the third and the fourth experiment, zero air
was humidified only for the zero air measurement and the NO measurement, respectively. We repeated the latter introducing a
lower relative humidity of $\sim 35\%$ and obtained the same result.

Figure 6 shows the temporal development of the background signal in ppbv in the NO_c channel after 2 h NO measurement with
365 a concentration of 16 ppbv. The red line shows the experiment under dry conditions and the blue line presents the experiment
under humid conditions. For the yellow line, we performed the NO measurement under dry conditions and the following back-
ground measurement under humid conditions. The green line shows humid NO measurement and dry background measure-
ment. Figure 6a presents the results obtained with the conventional blue light converter modified with a quartz glass cylinder.
All experiments showed a decreasing background signal over time in the NO_c channel. For comparison, the background signal
370 in the NO channel did not show a trend over time for any experiment which is presented in Figure S4 of the Supplement. This
indicates that the converter adsorbs NO molecules, for example during NO measurements, and desorbs them during zero air
measurements. At $t = 0$ min, the background signals for all experiments were approximately the same between 90 and 100 pptv,

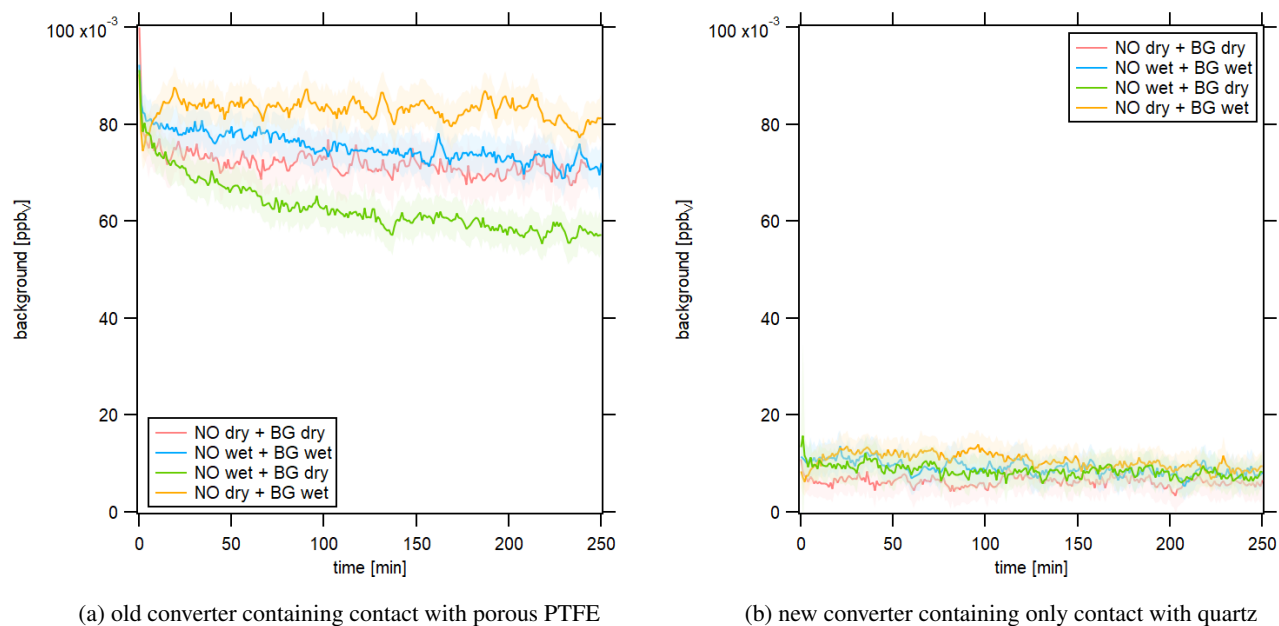


Figure 6. Instrumental background in response to dry and humid conditions after 2 h of NO calibration at 16 ppbv in the NO_c channel. The LEDs of the photolytic converter were switched on.

but showed a different development over time. The strongest decline by around 25 % over 250 minutes was observed for dry background measurement after humid NO measurement (green curve). For the opposite case, humid background measurement after dry NO measurement, the signal decreased by around 5 % over the observed time period (yellow curve). Performing the whole experiment under dry or humid conditions (red and blue curve, respectively) had a similar outcome with a background signal decrease of approximately 10 %. These observations indicate that the background measurements in the NO_c channel which were performed during CAFE Africa and used for the data processing according to Equation (4) were consistently too high as they were only run for two times one minute (per CB-cycle) and therefore did not represent the actual instrumental background but an artifact signal. In the laboratory, we observed the strongest effect for a dry background measurement following a humid NO measurement which was a likely scenario for the ambient monitoring during CAFE Africa as zero air for a background measurement was sampled from a gas cylinder (dry conditions) and the measured ambient concentration was subject to ambient meteorological conditions. This would explain the occurrence of negative NO_2 concentrations obtained from CLD measurements as mentioned earlier. These experiments also suggest that water molecules might not just promote adsorptive or desorptive processes, but participate in the surface allocation themselves and compete with NO. Following this hypothesis, the surface spaces would fill with NO during an NO measurement under dry conditions and with both, NO and H_2O molecules, under wet conditions. A subsequent background measurement under dry conditions would then lead to NO (and possibly H_2O) desorption. For a subsequent background measurement under humid conditions, H_2O molecules could actively replace NO molecules because of their higher surface affinity, leading to a temporally longer "leakage" of NO and a

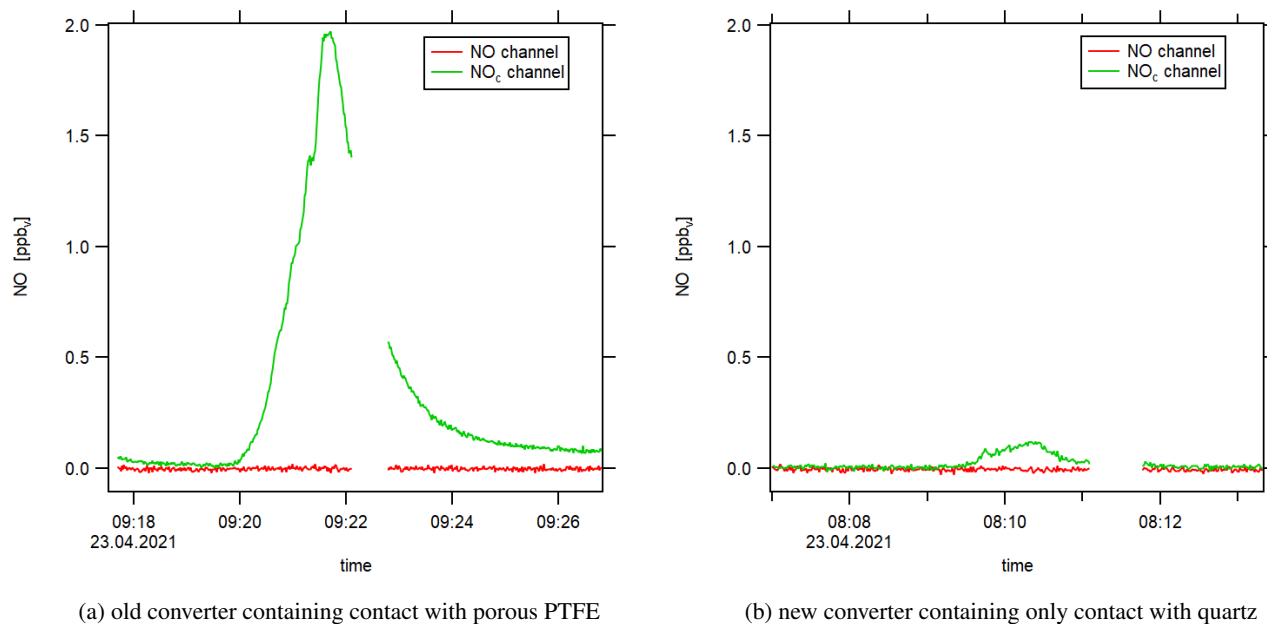


Figure 7. Instrumental background (zero air measurement) when heating the switched off photolytic converter with a heat gun. The small data gaps are due to prechamber measurements.

390 slower decrease in the background signal. The described effect would be highest for a dry NO measurement which gives the maximum NO surface coverage and a wet zero air measurement (yellow), while it would be lowest for the opposite case for which we observed the lowest background signal after 250 minutes (green). This hypothesis fits well with the observations during CAFE Africa presented in Section 3.1.3 where we observed a sharp increase in the NO_2 signal along with rapid increases in water vapor concentration. H_2O molecules could replace adsorbed NO molecules (or other atmospheric compounds) which were detected by the CLD as an artifact signal. Because of the conversion efficiency of 24.4 % of the blue light converter, the signal difference from the NO and the NO_c channel was multiplied by a factor of around four (compare Eq. (4)). Therefore, the resulting NO_2 signal was distorted by four times of the actual desorbed NO explaining the large peaks accompanying altitude descents.

We repeated the same laboratory experiments using the new photolytic converter. The resulting temporal development of the instrumental background is presented in Figure 6b which shows significant improvements compared to the conventional converter. The background in the NO_c channel was many times smaller for the new converter with mixing ratios of around 10 to 15 pptv and was, most importantly, constant over time. For stationary long-term experiments it could be possible to measure the instrumental background on the scale of hours. However for aircraft measurements and the accompanying rapid air mass changes due to the high aircraft velocity, it is vital to obtain a reliable background measurement within a short time interval, which would be possible with the new converter. Furthermore, changes in humidity did not seem to impact the measurement as all four experiments show the same result. This too, suggests the suitability of the new converter in



aircraft measurements or generally field studies which are impacted by high and changing humidities. Performing zero air measurements after NO₂ measurements had a similar outcome for each of the applied converters. The background measurement in the blue light converter showed a decreasing trend over time while it was constant and significantly smaller in the new
410 photolytic converter.

Our assumption that the observed effect is associated with NO molecules, not NO₂ molecules or other NO_x containing trace gases, is supported by an experiment where we heated the blue light converter with switched-off LEDs with a heat gun and observed a sharp increase in the NO_c channel during zero air measurement (following NO calibration measurement). The increase in temperature promoted the desorptive process and had to include NO molecules. Otherwise, the CLD would not have
415 detected any increase in the signal as the converters' LEDs were switched-off and NO₂ could not form NO via the photolytic reaction. We show the result of the heating experiment in Figure 7a. The converter surface was heated for two minutes (under constant movement of the heat gun) at a distance of around 10 cm during zero air measurement. We estimate the surface temperature to not have exceeded 200 °C. We observed a peak NO concentration of 2 ppbv (NO_c background was 0 ppbv). In comparison, Figure 7b shows the experiment repeated with the new quartz glass converter which showed a small increase in the
420 NO_c signal, too, but approximately one magnitude smaller compared to the conventional converter. The qualitative outcome of this experiment was the same with the LEDs switched-on as well as with preceding NO₂ (instead of NO) measurement. Please note that a direct comparison of experiments regarding adsorptive and desorptive processes with switched-on and -off LEDs is difficult because the operation of the LEDs increases the temperature within the converter which - as shown above - strongly impacts the surface allocation.

Beyond that, we performed an experiment to investigate how NO calibration measurements affect subsequent zero air measurements in response to different NO concentrations. Figure 8 shows the influence of the preceding NO concentration level on the following first 5 minutes of zero air measurement. We have performed 30 minute NO calibrations with NO concentrations between 0.25 ppbv and 10 ppbv. Red data points represent the background of the NO channel and green data points show the background of the NO_c channel. Background concentrations in the NO channel were independent of preceding NO concentrations. In contrast for the conventional converter, background concentrations in the NO_c channel increased with increasing NO
430 concentrations and leveled off for high values as shown in Figure 8a. Measured NO concentrations during CAFE Africa were between 0 and 1 ppbv and were therefore situated in the rising part of the curve. That shows that background measurements during CAFE Africa were not only too high, but also depended on the preceding NO concentration. We tried to retrospectively correct the NO₂ data with a lower instrumental background as obtained from laboratory investigations after several hours of
435 zero air sampling. However, it was not possible to quantify the effect of varying, preceding NO levels. Additionally, the impact of humidity had the exact opposite effect on the NO₂ measurements. While the higher than actual instrumental background led to lower than actual NO₂ concentrations, increases in humidity triggered higher than actual NO₂ concentrations. Figure 8b shows that the development of the background in the NO_c channel did not depend on the preceding NO concentrations for the new photolytic converter. The instrumental background was 12 ± 1 pptv and constant over the whole experiment. The detected
440 background signal for the NO_c channel disappeared when switching off the light of the UV-LEDs. A possible explanation can be a trace concentration of NO₂ in the utilized synthetic air as mentioned earlier.

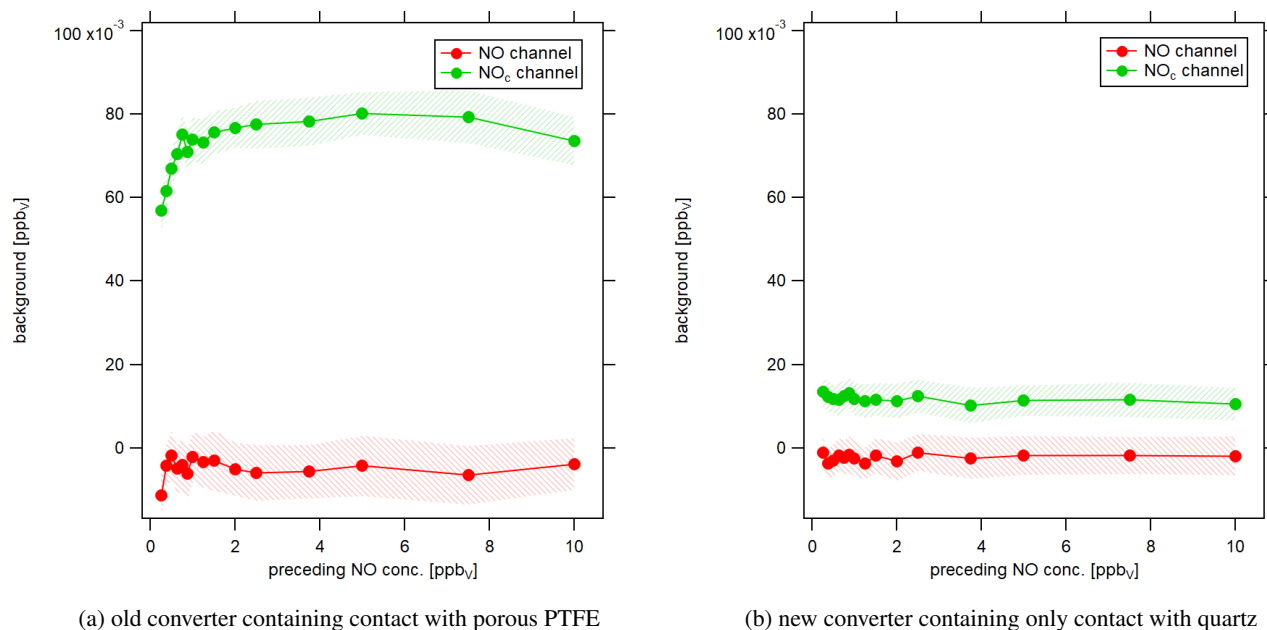


Figure 8. Instrumental background in response to different preceding NO concentrations under dry conditions. Each data point shows the level of the signal of the first 5 minutes of background measurements after NO calibrations.

While we have shown above that NO and humidity strongly affect the background measurements in the conventional blue light converter, it is likely that there are other factors contributing to the observed effects, too. When switching off the LEDs in the conventional converter, the observed instrumental background decreased rapidly (too rapidly for a sole temperature effect) which we present in Figure S5 of the Supplement. This suggests that the light of the LEDs impacts the instrumental background in the NO_c channel. Many other compounds can be photolyzed to form NO, such as PAN, ClNO_2 or BrONO_2 . However, their absorption cross sections suggest no interference at 398 nm, the spectral output maximum of the LEDs (Reed et al., 2016; Pollack et al., 2010). Only small interference could occur with HONO and NO_3 at the edge of the spectral output and this would require the presence of these compounds in the converter which should not be the case for the described laboratory investigations, but is conceivable given the memory effect observations. We have performed an uptake experiment for HNO_3 (nitric acid) to investigate the adsorptive capacity of the converters. HNO_3 in zero air (2500 sccm) was first routed through a bypass and after reaching a constant signal, the gas flow was changed to include the converter. The HNO_3 concentration behind the converter was monitored via chemical ionization mass spectrometry (CIMS). Figure S6a and S6b of the Supplement show the resulting adsorption behavior for the old and the new converter, respectively. When directing the gas flow through the old converter, the detected HNO_3 flux decreased rapidly by around a factor of four and we did not observe the signal return to its initial value within 40 minutes (which is when we terminated the experiment). This indicates a high absorptive capacity or a decay of HNO_3 in the converter (or both). Integration of the HNO_3 flux shows that the converter took up approximately 1.7×10^{16} HNO_3 molecules in the considered time frame. In contrast for the new converter, the HNO_3 flux decreased, too, but



returned to its initial value within 10 minutes while it adsorbed only $\sim 1.7 \times 10^{15}$ HNO₃ molecules. The observed adsorption capacity can be minimized by coating the quartz surface with FEP (fluorinated ethylene propylene) which provides a highly hydrophobic surface (Neuman et al., 1999; Liebmann et al., 2017). The number of adsorbed HNO₃ molecules was by a factor of 4 - 5 smaller compared to the non-coated quartz converter (Figure S6c). We did not observe any differences between the coated and the non-coated quartz converter regarding the experiments investigating the role of NO and humidity presented above. This uptake experiment shows the high adsorptive capacity of the old converter in comparison to the new quartz converter. In the case of HNO₃, which could have been adsorbed by the converter e.g. during stratospheric measurements, we hypothesize a potential source of NO or NO₂ through for example surface-catalyzed chemistry, possibly involving the light of the LEDs or elevated temperature. Again, this experiment underlines the superiority of the new photolytic converter over the conventional blue light converter and suggests the applicability for ambient and airborne measurements.

4 Conclusions

In this study, we have investigated a modified conventional blue light converter with a highly reflective and porous inner surface made from optical PTFE regarding its application during the research aircraft campaign CAFE Africa which took place in August and September 2018 around Cabo Verde. We have identified a memory effect in the blue light converter which is affected by humidity, especially by rapid changes in water vapor concentrations, as well as preceding NO levels, which is particularly relevant for the low NO₂/NO ratio in the upper troposphere. The high adsorptive capacity regarding other atmospheric trace gases such as HNO₃ and the light of the LEDs could additionally play a role in the observed effects. Because of the complex correlations between these parameters it is not possible to retrospectively correct the NO₂ signal measured during CAFE Africa to receive reliable data. Instead, we suggest the application of a new photolytic converter made from quartz glass in order to prevent the gas flow from contact with the porous PTFE surface which can additionally be coated with FEP to obtain highly hydrophobic properties. Laboratory results indicate a high suitability of the newly developed converter in aircraft measurements which - looking into the future - should be investigated in detail in order to improve in-field NO₂ measurements. With an improved instrumental background, other important questions of current atmospheric NO₂ research such as deviations from photostationary state NO₂ in remote locations or interferences from NO_y species could be addressed and investigated more easily.

Data availability. Data measured during the flight campaign CAFE Africa are available to all scientists agreeing to the CAFE Africa data protocol.

Author contributions. HF had the idea. CMN and HF designed the study. CMN analyzed the data and wrote the manuscript. CMN performed the laboratory experiments. CMN, UP and HF designed the new photolytic converter. IT provided CLD NO_x, CO and CH₄ data for CAFE Africa. Photolysis frequencies were received from BB. DM, MM, RR and HH measured and provided the OH and HO₂ data. KP ad FK



490 measured and provided the NO₂ miniDOAS data. FO measured and provided the O₃ data. H₂O data were received from MZ. RD and JNC measured and provided the PAN data. HF, JL and HH had a large contribution in the operation and planning of the aircraft campaign.

Competing interests. Hartwig Harder is a member of the editorial board of the journal.

Acknowledgements. We acknowledge the collaboration with the DLR (German Aerospace Center) during CAFE Africa. This work was supported by the Max Planck Graduate Center with the Johannes Gutenberg-Universität Mainz (MPGC). FK and KP acknowledge the support given by the Deutsche Forschungsgemeinschaft (DFG) through the projects PF 384-16, PF 384-17, and PF 384-19.

495 *Financial support.* The article processing charges for this open access publication were covered by the Max Planck Society.



References

- Alam, M. S., Crilley, L. R., Lee, J. D., Kramer, L. J., Pfrang, C., Vázquez-Moreno, M., Ródenas, M., Muñoz, A., and Bloss, W. J.: Interference from alkenes in chemiluminescent NO_x measurements, *Atmospheric Measurement Techniques*, 13, 5977–5991, <https://doi.org/10.5194/amt-13-5977-2020>, 2020.
- 500 Andersen, S. T., Carpenter, L. J., Nelson, B. S., Neves, L., Read, K. A., Reed, C., Ward, M., Rowlinson, M. J., and Lee, J. D.: Long-term NO_x measurements in the remote marine tropical troposphere, *Atmospheric Measurement Techniques Discussions* [preprint], pp. 1–34, <https://doi.org/10.5194/amt-2020-469>, in review, 2020.
- Atkinson, R., Baulch, D., Cox, R., Crowley, J., Hampson, R., Hynes, R., Jenkin, M., Rossi, M., and Troe, J.: Evaluated kinetic and photochemical data for atmospheric chemistry: Volume I-gas phase reactions of O_x, HO_x, NO_x and SO_x species, *Atmospheric chemistry and physics*, 4, 1461–1738, <https://doi.org/10.5194/acp-4-1461-2004>, 2004.
- 505 Atkinson, R., Baulch, D., Cox, R., Crowley, J., Hampson, R., Hynes, R., Jenkin, M., Rossi, M., Troe, J., and Subcommittee, I.: Evaluated kinetic and photochemical data for atmospheric chemistry: Volume II-gas phase reactions of organic species, *Atmospheric chemistry and physics*, 6, 3625–4055, <https://doi.org/10.5194/acp-6-3625-2006>, 2006.
- Bahta, A., Simonaitis, R., and Heicklen, J.: Thermal decomposition kinetics of methyl peroxyxynitrate (CH₃O₂NO₂), *The Journal of Physical Chemistry*, 86, 1849–1853, 1982.
- 510 Bohn, B. and Lohse, I.: Calibration and evaluation of CCD spectroradiometers for ground-based and airborne measurements of spectral actinic flux densities, *Atmospheric measurement techniques*, 10, 3151–3174, <https://doi.org/10.5194/amt-10-3151-2017>, 2017.
- Boningari, T. and Smirniotis, P. G.: Impact of nitrogen oxides on the environment and human health: Mn-based materials for the NO_x abatement, *Current Opinion in Chemical Engineering*, 13, 133–141, <https://doi.org/10.1016/j.coche.2016.09.004>, 2016.
- 515 Bozem, H., Butler, T. M., Lawrence, M. G., Harder, H., Martinez, M., Kubistin, D., Lelieveld, J., and Fischer, H.: Chemical processes related to net ozone tendencies in the free troposphere, *Atmospheric Chemistry and Physics*, 17, 10 565–10 582, <https://doi.org/10.5194/acp-17-10565-2017>, 2017.
- Breuninger, C., Meixner, F. X., and Kesselmeier, J.: Field investigations of nitrogen dioxide (NO₂) exchange between plants and the atmosphere, *Atmospheric Chemistry and Physics*, 13, 773–790, <https://doi.org/10.5194/acp-13-773-2013>, 2013.
- 520 Browne, E., Perring, A., Wooldridge, P., Apel, E., Hall, S., Huey, L., Mao, J., Spencer, K., St Clair, J., Weinheimer, A., Wisthaler, A., and Cohen, R. C.: Global and regional effects of the photochemistry of CH₃O₂NO₂: evidence from ARCTAS, *Atmospheric Chemistry and Physics*, 11, 4209–4219, <https://doi.org/10.5194/acp-11-4209-2011>, 2011.
- Clough, P. and Thrush, B. A.: Mechanism of chemiluminescent reaction between nitric oxide and ozone, *Transactions of the Faraday Society*, 63, 915–925, <https://doi.org/10.1039/TF9676300915>, 1967.
- 525 Crowley, J., Schuster, G., Pouvesle, N., Parchatka, U., Fischer, H., Bonn, B., Bingemer, H., and Lelieveld, J.: Nocturnal nitrogen oxides at a rural mountain-site in south-western Germany, *Atmospheric Chemistry and Physics*, 10, 2795–2812, <https://doi.org/10.5194/acp-10-2795-2010>, 2010.
- Demerjian, K. L.: A review of national monitoring networks in North America, *Atmospheric Environment*, 34, 1861–1884, [https://doi.org/10.1016/S1352-2310\(99\)00452-5](https://doi.org/10.1016/S1352-2310(99)00452-5), 2000.
- 530 ECO PHYSICS AG: CLD 790 SR User-Manual, 2002.



- Fischer, E., Jacob, D. J., Yantosca, R. M., Sulprizio, M. P., Millet, D., Mao, J., Paulot, F., Singh, H., Roiger, A., Ries, L., et al.: Atmospheric peroxyacetyl nitrate (PAN): a global budget and source attribution, *Atmospheric Chemistry and Physics*, 14, 2679–2698, <https://doi.org/10.5194/acp-14-2679-2014>, 2014.
- 535 Frey, M., Roscoe, H., Kukui, A., Savarino, J., France, J., King, M., Legrand, M., and Preunkert, S.: Atmospheric nitrogen oxides (NO and NO₂) at Dome C, East Antarctica, during the OPALE campaign, *Atmospheric Chemistry and Physics*, 15, 7859–7875, <https://doi.org/10.5194/acp-15-7859-2015>, 2015.
- Fuchs, H., Ball, S. M., Bohn, B., Brauers, T., Cohen, R., Dorn, H.-P., Dubé, W., Fry, J., Häsel, R., Heitmann, U., Jones, R. L., Kleffmann, J., Mentel, T. F., Musgen, P., Rohrer, F., Rollins, A. W., Ruth, A. A., Kiendler-Scharr, A., Schlosser, E., Shillings, A. J. L., Tillmann, R., Varma, R. M., Venables, D. S., Tapia, G. V., Wahner, A., Wegener, R., Wooldridge, P. J., and Brown, S. S.: Intercomparison of
540 measurements of NO₂ concentrations in the atmosphere simulation chamber SAPHIR during the NO₃Comp campaign, *Atmospheric Measurement Techniques*, 3, 21–37, <https://doi.org/10.5194/amt-3-21-2010>, 2010.
- Ganzeveld, L., Lelieveld, J., Dentener, F., Krol, M., Bouwman, A., and Roelofs, G.-J.: Global soil-biogenic NO_x emissions and the role of canopy processes, *Journal of Geophysical Research: Atmospheres*, 107, ACH-9, <https://doi.org/10.1029/2001JD000684>, 2002.
- 545 Ge, B., Sun, Y., Liu, Y., Dong, H., Ji, D., Jiang, Q., Li, J., and Wang, Z.: Nitrogen dioxide measurement by cavity attenuated phase shift spectroscopy (CAPS) and implications in ozone production efficiency and nitrate formation in Beijing, China, *Journal of Geophysical Research: Atmospheres*, 118, 9499–9509, <https://doi.org/10.1002/jgrd.50757>, 2013.
- Greaver, T. L., Sullivan, T. J., Herrick, J. D., Barber, M. C., Baron, J. S., Cosby, B. J., Deerpake, M. E., Dennis, R. L., Dubois, J.-J. B., Goodale, C. L., et al.: Ecological effects of nitrogen and sulfur air pollution in the US: what do we know?, *Frontiers in Ecology and the Environment*, 10, 365–372, <https://doi.org/10.1890/110049>, 2012.
- 550 Griffin, R. J., Beckman, P. J., Talbot, R. W., Sive, B. C., and Varner, R. K.: Deviations from ozone photostationary state during the International Consortium for Atmospheric Research on Transport and Transformation 2004 campaign: Use of measurements and photochemical modeling to assess potential causes, *Journal of Geophysical Research: Atmospheres*, 112, <https://doi.org/10.1029/2006JD007604>, 2007.
- Hosaynali Beygi, Z., Fischer, H., Harder, H., Martinez, M., Sander, R., Williams, J., Brookes, D., Monks, P., and Lelieveld, J.: Oxidation photochemistry in the Southern Atlantic boundary layer: unexpected deviations of photochemical steady state, *Atmospheric Chemistry and Physics*, 11, 8497–8513, <https://doi.org/10.5194/acp-11-8497-2011>, 2011.
- 555 Hüneke, T., Aderhold, O.-A., Bounin, J., Dorf, M., Gentry, E., Grossmann, K., Groß, J.-U., Hoor, P., Jöckel, P., Kenntner, M., Knapp, M., Knecht, M., Lörks, D., Ludmann, S., Matthes, S., Raecke, R., Reichert, M., Weimar, J., Werner, B., Zahn, A., Ziereis, H., and Pfeilsticker, K.: The novel HALO mini-DOAS instrument: inferring trace gas concentrations from airborne UV/visible limb spectroscopy under all skies using the scaling method, *Atmospheric Measurement Techniques*, 10, 4209–4234, <https://doi.org/10.5194/amt-10-4209-2017>, 2017.
- 560 IUPAC Task Group on Atmospheric Chemical Kinetic Data Evaluation: Evaluated Kinetic Data, <http://iupac.pole-ether.fr>, "accessed on 2021-02-02", 2021.
- Jacob, D. J.: Introduction to atmospheric chemistry, Princeton University Press, 1999.
- Javed, U., Kubistin, D., Martinez, M., Pollmann, J., Rudolf, M., Parchatka, U., Reiffs, A., Thieser, J., Schuster, G., Horbanski, M., et al.: Laser-induced fluorescence-based detection of atmospheric nitrogen dioxide and comparison of different techniques during the PARADE
565 2011 field campaign, *Atmospheric Measurement Techniques*, 12, 1461–1481, <https://doi.org/10.5194/amt-12-1461-2019>, 2019.
- Jordan, N., Garner, N. M., Matchett, L. C., Tokarek, T. W., Osthoff, H. D., Odame-Ankrah, C. A., Grimm, C. E., Pickrell, K. N., Swainson, C., and Rosentreter, B. W.: Potential interferences in photolytic nitrogen dioxide converters for ambient air monitoring: Evaluation of a prototype, *Journal of the Air & Waste Management Association*, 70, 753–764, <https://doi.org/10.1080/10962247.2020.1769770>, 2020.



- Jung, J., Lee, J., Kim, B., and Oh, S.: Seasonal variations in the NO₂ artifact from chemiluminescence measurements with a molybdenum converter at a suburban site in Korea (downwind of the Asian continental outflow) during 2015–2016, *Atmospheric Environment*, 165, 290–300, <https://doi.org/10.1016/j.atmosenv.2017.07.0101352-2310>, 2017.
- Kaufmann, S., Voigt, C., Heller, R., Jurkat-Witschas, T., Krämer, M., Rolf, C., Zöger, M., Giez, A., Buchholz, B., Ebert, V., Thornberry, T., and Schumann, U.: Intercomparison of midlatitude tropospheric and lower-stratospheric water vapor measurements and comparison to ECMWF humidity data, *Atmospheric chemistry and physics*, 18, 16 729–16 745, <https://doi.org/10.5194/acp-18-16729-2018>, 2018.
- 575 Keababian, P. L., Herndon, S. C., and Freedman, A.: Detection of nitrogen dioxide by cavity attenuated phase shift spectroscopy, *Analytical chemistry*, 77, 724–728, <https://doi.org/10.1021/ac048715y>, 2005.
- Kim, S., Huey, L. G., Stickel, R., Tanner, D., Crawford, J. H., Olson, J. R., Chen, G., Brune, W., Ren, X., Leshner, R., Wooldridge, P. J., Bertram, T. H., Perring, A., Cohen, R. C., Lefer, B. L., Shetter, R. E., Avery, M., Diskin, G., and Sokolik, I.: Measurement of HO₂NO₂ in the free troposphere during the Intercontinental Chemical Transport Experiment–North America 2004, *Journal of Geophysical Research: Atmospheres*, 112, <https://doi.org/10.1029/2006JD007676>, 2007.
- 580 Kluge, F., Hüneke, T., Knecht, M., Lichtenstern, M., Rotermund, M., Schlager, H., Schreiner, B., and Pfeilsticker, K.: Profiling of formaldehyde, glyoxal, methylglyoxal, and CO over the Amazon: normalized excess mixing ratios and related emission factors in biomass burning plumes, *Atmospheric Chemistry and Physics*, 20, 12 363–12 389, <https://doi.org/10.5194/acp-20-12363-2020>, 2020.
- Lee, J., Moller, S., Read, K., Lewis, A., Mendes, L., and Carpenter, L.: Year-round measurements of nitrogen oxides and ozone in the tropical North Atlantic marine boundary layer, *Journal of Geophysical Research: Atmospheres*, 114, <https://doi.org/10.1029/2009JD011879>, 2009.
- 585 Leighton, P.: *Photochemistry of air pollution*, Academic Press, Inc., 1961.
- Lelieveld, J. and Dentener, F. J.: What controls tropospheric ozone?, *Journal of Geophysical Research: Atmospheres*, 105, 3531–3551, <https://doi.org/10.1029/1999JD901011>, 2000.
- Levy, H.: Normal atmosphere: Large radical and formaldehyde concentrations predicted, *Science*, 173, 141–143, <https://doi.org/10.1126/science.173.3992.141>, 1971.
- 590 Liebmann, J. M., Schuster, G., Schuladen, J. B., Sobanski, N., Lelieveld, J., and Crowley, J. N.: Measurement of ambient NO₃ reactivity: design, characterization and first deployment of a new instrument, *Atmospheric Measurement Techniques*, 10, 1241–1258, <https://doi.org/10.5194/amt-10-1241-2017>, 2017.
- Lippmann, M.: Health effects of ozone a critical review, *Japca*, 39, 672–695, <https://doi.org/10.1080/08940630.1989.10466554>, 1989.
- 595 Logan, J. A.: Nitrogen oxides in the troposphere: Global and regional budgets, *Journal of Geophysical Research: Oceans*, 88, 10 785–10 807, <https://doi.org/10.1029/JC088iC15p10785>, 1983.
- Logan, J. A., Prather, M. J., Wofsy, S. C., and McElroy, M. B.: Tropospheric chemistry: A global perspective, *Journal of Geophysical Research: Oceans*, 86, 7210–7254, <https://doi.org/10.1029/JC086iC08p07210>, 1981.
- Ma, Y., Lu, K., Chou, C. C.-K., Li, X., and Zhang, Y.: Strong deviations from the NO-NO₂-O₃ photostationary state in the Pearl River Delta: Indications of active peroxy radical and chlorine radical chemistry, *Atmospheric Environment*, 163, 22–34, <https://doi.org/10.1016/j.atmosenv.2017.05.012>, 2017.
- 600 Mannschreck, K., Gilge, S., Plass-Duelmer, C., Fricke, W., and Berresheim, H.: Assessment of the applicability of NO-NO₂-O₃ photostationary state to long-term measurements at the Hohenpeissenberg GAW Station, Germany, *Atmospheric Chemistry and Physics*, 4, 1265–1277, <https://doi.org/10.5194/acp-4-1265-2004>, 2004.



- 605 Marno, D., Ernest, C., Hens, K., Javed, U., Klimach, T., Martinez, M., Rudolf, M., Lelieveld, J., and Harder, H.: Calibration of an airborne HO_x instrument using the All Pressure Altitude-based Calibrator for HO_x Experimentation (APACHE), *Atmospheric Measurement Techniques*, 13, 2711–2731, <https://doi.org/10.5194/amt-13-2711-2020>, 2020.
- Murphy, J., Thornton, J., Wooldridge, P., Day, D., Rosen, R., Cantrell, C., Shetter, R., Lefer, B., and Cohen, R.: Measurements of the sum of HO₂NO₂ and CH₃O₂NO₂ in the remote troposphere, *Atmospheric Chemistry and Physics*, 4, 377–384, <https://doi.org/10.5194/acp-4-377-2004>, 2004.
- 610 Nault, B., Garland, C., Pusede, S., Wooldridge, P., Ullmann, K., Hall, S., and Cohen, R.: Measurements of CH₃O₂NO₂ in the upper troposphere, *Atmospheric Measurement Techniques*, 8, 987–997, <https://doi.org/10.5194/amt-8-987-2015>, 2015.
- Neuman, J., Huey, L., Ryerson, T., and Fahey, D.: Study of inlet materials for sampling atmospheric nitric acid, *Environmental Science & Technology*, 33, 1133–1136, <https://doi.org/10.1021/es980767f>, 1999.
- 615 Novelli, A., Hens, K., Tatum Ernest, C., Kubistin, D., Regelin, E., Elste, T., Plass-Dülmer, C., Martinez, M., Lelieveld, J., and Harder, H.: Characterisation of an inlet pre-injector laser-induced fluorescence instrument for the measurement of atmospheric hydroxyl radicals, *Atmospheric measurement techniques*, 7, 3413–3430, <https://doi.org/10.5194/amt-7-3413-2014>, 2014.
- Nussbaumer, C. M. and Cohen, R. C.: The Role of Temperature and NO_x in Ozone Trends in the Los Angeles Basin, *Environmental Science & Technology*, 54, 15 652–15 659, <https://doi.org/10.1021/acs.est.0c04910>, 2020.
- 620 Nussbaumer, C. M., Tadic, I., Dienhart, D., Wang, N., Edtbauer, A., Ernle, L., Williams, J., Obersteiner, F., Gutiérrez-Álvarez, I., Harder, H., Lelieveld, J., and Fischer, H.: Measurement report: In situ observations of deep convection without lightning during the tropical cyclone Florence 2018, *Atmospheric Chemistry and Physics*, 21, 7933–7945, <https://doi.org/10.5194/acp-2021-79>, 2021.
- Nuvolone, D., Petri, D., and Voller, F.: The effects of ozone on human health, *Environmental Science and Pollution Research*, 25, 8074–8088, <https://doi.org/10.1007/s11356-017-9239-3>, 2018.
- 625 O’Keefe, A. and Deacon, D. A.: Cavity ring-down optical spectrometer for absorption measurements using pulsed laser sources, *Review of scientific instruments*, 59, 2544–2551, <https://doi.org/10.1063/1.1139895>, 1988.
- Phillips, G., Pouvesle, N., Thieser, J., Schuster, G., Axinte, R., Fischer, H., Williams, J., Lelieveld, J., and Crowley, J.: Peroxyacetyl nitrate (PAN) and peroxyacetic acid (PAA) measurements by iodide chemical ionisation mass spectrometry: first analysis of results in the boreal forest and implications for the measurement of PAN fluxes, *Atmospheric Chemistry and Physics*, 13, 1129–1139, <https://doi.org/10.5194/acp-13-1129-2013>, 2013.
- 630 Pollack, I. B., Lerner, B. M., and Ryerson, T. B.: Evaluation of ultraviolet light-emitting diodes for detection of atmospheric NO₂ by photolysis-chemiluminescence, *Journal of Atmospheric Chemistry*, 65, 111–125, <https://doi.org/10.1007/s10874-011-9184-3>, 2010.
- Pusede, S. E., Steiner, A. L., and Cohen, R. C.: Temperature and recent trends in the chemistry of continental surface ozone, *Chemical reviews*, 115, 3898–3918, <https://doi.org/10.1021/cr5006815>, 2015.
- 635 Reed, C., Evans, M. J., Carlo, P. D., Lee, J. D., and Carpenter, L. J.: Interferences in photolytic NO₂ measurements: explanation for an apparent missing oxidant?, *Atmospheric Chemistry and Physics*, 16, 4707–4724, <https://doi.org/10.5194/acp-16-4707-2016>, 2016.
- Reidmiller, D., Jaffe, D., Fischer, E., and Finley, B.: Nitrogen oxides in the boundary layer and free troposphere at the Mt. Bachelor Observatory, *Atmospheric Chemistry and Physics*, 10, 6043–6062, <https://doi.org/10.5194/acp-10-6043-2010>, 2010.
- Ridley, B. and Howlett, L.: An instrument for nitric oxide measurements in the stratosphere, *Review of Scientific Instruments*, 45, 742–746, <https://doi.org/10.1063/1.1686726>, 1974.
- 640 Ryerson, T., Williams, E., and Fehsenfeld, F.: An efficient photolysis system for fast-response NO₂ measurements, *Journal of Geophysical Research: Atmospheres*, 105, 26 447–26 461, <https://doi.org/10.1029/2000JD900389>, 2000.



- Sadanaga, Y., Fukumori, Y., Kobashi, T., Nagata, M., Takenaka, N., and Bandow, H.: Development of a selective light-emitting diode photolytic NO₂ converter for continuously measuring NO₂ in the atmosphere, *Analytical chemistry*, 82, 9234–9239, <https://doi.org/10.1021/ac101703z>, 2010.
- 645 Sather, M. E., Slonecker, E. T., Kronmiller, K. G., Williams, D. D., Daughtrey, H., and Mathew, J.: Evaluation of short-term Ogawa passive, photolytic, and federal reference method sampling devices for nitrogen oxides in El Paso and Houston, Texas, *Journal of Environmental Monitoring*, 8, 558–563, <https://doi.org/10.1039/b601113f>, 2006.
- Schiller, C., Bozem, H., Gurk, C., Parchatka, U., Königstedt, R., Harris, G., Lelieveld, J., and Fischer, H.: Applications of quantum cascade lasers for sensitive trace gas measurements of CO, CH₄, N₂O and HCHO, *Applied Physics B*, 92, 419–430, 2008.
- 650 Silvern, R., Jacob, D., Travis, K., Sherwen, T., Evans, M., Cohen, R., Laughner, J., Hall, S., Ullmann, K., Crouse, J., Wennberg, P. O., Peischl, J., and Pollack, I. B.: Observed NO/NO₂ ratios in the upper troposphere imply errors in NO-NO₂-O₃ cycling kinetics or an unaccounted NO_x reservoir, *Geophysical Research Letters*, 45, 4466–4474, <https://doi.org/10.1029/2018GL077728>, 2018.
- SphereOptics GmbH: Introduction Diffuse Reflecting Materials, https://sphereoptics.de/en/product/introduction-diffuse-reflecting-materials/?gclid=EAIaIQobChMI9cGJkfH87AIVjql3Ch2jMQ0TEAAYASAAEgJSyvD_BwE, "accessed on 2021-02-02", 2017.
- 655 Tadic, I., Crowley, J. N., Dienhart, D., Eger, P., Harder, H., Hottmann, B., Martinez, M., Parchatka, U., Paris, J.-D., Pozzer, A., Rohloff, R., Schuladen, J., Shenolikar, J., Tauer, S., Lelieveld, J., and Fischer, H.: Net ozone production and its relationship to nitrogen oxides and volatile organic compounds in the marine boundary layer around the Arabian Peninsula, *Atmospheric Chemistry and Physics*, 20, 6769–6787, <https://doi.org/10.5194/acp-20-6769-2020>, 2020.
- 660 Tadic, I., Nussbaumer, C., Bohn, B., Harder, H., Marno, D., Martinez, M., Obersteiner, F., Parchatka, U., Pozzer, A., Rohloff, R., Zöger, M., Lelieveld, J., and Fischer, H.: Central role of nitric oxide in ozone production in the upper tropical troposphere over the Atlantic Ocean and West Africa, *Atmospheric Chemistry and Physics*, 21, 8195–8211, <https://doi.org/10.5194/acp-2021-52>, 2021.
- Thornton, J. A., Wooldridge, P. J., and Cohen, R. C.: Atmospheric NO₂: In situ laser-induced fluorescence detection at parts per trillion mixing ratios, *Analytical Chemistry*, 72, 528–539, <https://doi.org/10.1021/ac9908905>, 2000.
- 665 Travis, K. R., Jacob, D. J., Fisher, J. A., Kim, P. S., Marais, E. A., Zhu, L., Yu, K., Miller, C. C., Yantosca, R. M., Sulprizio, M. P., Thompson, A. M., Wennberg, P. O., Crouse, J. D., Clair, J. M. S., Cohen, R. C., Laughner, J. L., Dibb, J. E., Hall, S. R., Ullmann, K., Wolfe, G. M., Pollack, I. B., Peischl, J., Neuman, J. A., and Zhou, X.: Why do models overestimate surface ozone in the Southeast United States?, *Atmospheric Chemistry and Physics*, 16, 13 561–13 577, <https://doi.org/10.5194/acp-16-13561-2016>, 2016.
- Ventrillard, I., Gorrotxategi-Carbajo, P., and Romanini, D.: Part per trillion nitric oxide measurement by optical feedback cavity-enhanced absorption spectroscopy in the mid-infrared, *Applied Physics B*, 123, 1–8, <https://doi.org/10.1007/s00340-017-6750-7>, 2017.
- 670 Veres, P., Roberts, J., Wild, R., Edwards, P., Brown, S., Bates, T., Quinn, P., Johnson, J., Zamora, R., and de Gouw, J.: Peroxynitric acid (HO₂NO₂) measurements during the UBWOS 2013 and 2014 studies using iodide ion chemical ionization mass spectrometry, *Atmospheric Chemistry and Physics*, 15, 8101–8114, <https://doi.org/10.5194/acp-15-8101-2015>, 2015.
- Villena, G., Bejan, I., Kurtenbach, R., Wiesen, P., and Kleffmann, J.: Interferences of commercial NO₂ instruments in the urban atmosphere and in a smog chamber, *Atmospheric Measurement Techniques*, 5, 149–159, <https://doi.org/10.5194/amt-5-149-2012>, 2012.
- Westfalen Gas Schweiz GmbH: Synth. Luft, KW frei T50 MFI, <https://shop.westfalen.com/ch/de/Home/Gase/Sondergase/Synthetische-Luft-KW-frei/p/S09110150>, "accessed on 2021-03-26".
- Winer, A. and Biermann, H.: Long pathlength differential optical absorption spectroscopy (DOAS) measurements of gaseous HONO, NO₂ and HCNO in the California South Coast Air Basin, *Research on Chemical Intermediates*, 20, 423–445, 1994.



- 680 Xu, Z., Wang, T., Xue, L., Louie, P. K., Luk, C. W., Gao, J., Wang, S., Chai, F., and Wang, W.: Evaluating the uncertainties of thermal catalytic conversion in measuring atmospheric nitrogen dioxide at four differently polluted sites in China, *Atmospheric Environment*, 76, 221–226, <https://doi.org/10.1016/j.atmosenv.2012.09.043>, 2013.
- Zahn, A., Weppner, J., Widmann, H., Schlote-Holubek, K., Burger, B., Kühner, T., and Franke, H.: A fast and precise chemiluminescence ozone detector for eddy flux and airborne application, *Atmospheric Measurement Techniques*, 5, 363–375, <https://doi.org/10.5194/amt-5-363-2012>, 2012.
- 685 Zheng, K., Zheng, C., Zhang, Y., Wang, Y., and Tittel, F. K.: Review of incoherent broadband cavity-enhanced absorption spectroscopy (IBBCEAS) for gas sensing, *Sensors*, 18, 3646, <https://doi.org/10.3390/s18113646>, 2018.